Precise Measurement of Deuteron Tensor Analyzing Powers with BLAST

C. Zhang,[1] M. Kohl,[2,*] T. Akdogan,[1] R. Alarcon,[3] W. Bertozzi,[1] E. Booth,[4] T. Botto,[1] J. R. Calarco,[5] B. Clasie,[1] C. Crawford,[6] A. DeGrush,[1] K. Dow,[1] M. Farkhondeh,[1] R. Fatemi,[6] O. Filoti,[5] W. Franklin,[1] H. Gao,[7] E. Geis,[3] S. Gilad,[1] D. Hasell,[1] P. Karpius,[5] H. Kolster,[1] T. Lee,[5] A. Maschinot,[1] J. Matthews,[1] K. McIlhany,[8] N. Meitanis,[1] R. Milner,[1] J. Rapaport,[9] R. Redwine,[1] J. Seely,[1] A. Shinozaki,[1] A. Sindile,[5] S. Širca,[10] E. Six,[3] T. Smith,[11] B. Tonguc,[3] C. Tschalär,[1] E. Tsentalovich,[1] W. Turchinetz,[1] Y. Xiao,[1] W. Xu,[7] Z.-L. Zhou,[1] V. Ziskin,[1] and T. Zwart[1]

(The BLAST collaboration)

[1]*Laboratory for Nuclear Science and Bates Linear Accelerator Center, Massachusetts Institute of Technology, Cambridge, Massachusetts 02139, USA*
[2]*Hampton University, Hampton, Virginia 23668 and Thomas Jefferson National Accelerator Facility, Newport News, Virginia 23606, USA*
[3]*Arizona State University, Tempe, Arizona 85287, USA*
[4]*Boston University, Boston, Massachusetts 02215, USA*
[5]*University of New Hampshire, Durham, New Hampshire 03824, USA*
[6]*University of Kentucky, Lexington, Kentucky 40504, USA*
[7]*Triangle Universities Nuclear Laboratory and Duke University, Durham, North Carolina 27708, USA*
[8]*United States Naval Academy, Annapolis, Maryland 21402, USA*
[9]*Ohio University, Athens, Ohio 45701, USA*
[10]*Institute "Jožef Stefan," University of Ljubljana, SI-1001 Ljubljana, Slovenia*
[11]*Dartmouth College, Hanover, New Hampshire 03755, USA*
(Received 21 September 2011; published 13 December 2011)

We report a precision measurement of the deuteron tensor analyzing powers T_{20} and T_{21} at the MIT-Bates Linear Accelerator Center. Data were collected simultaneously over a momentum transfer range $Q = 2.15$–4.50 fm^{-1} with the Bates Large Acceptance Spectrometer Toroid using a highly polarized deuterium internal gas target. The data are in excellent agreement with calculations in a framework of effective field theory. The deuteron charge monopole and quadrupole form factors G_C and G_Q were separated with improved precision, and the location of the first node of G_C was confirmed at $Q = 4.19 \pm 0.05$ fm^{-1}. The new data provide a strong constraint on theoretical models in a momentum transfer range covering the minimum of T_{20} and the first node of G_C.

DOI: 10.1103/PhysRevLett.107.252501 PACS numbers: 25.30.Bf, 13.40.Gp, 13.88.+e

The deuteron, as the only two-nucleon bound state, plays an important role in the understanding of nucleon-nucleon interactions including short-range properties and non-nucleonic degrees of freedom [1–3]. During the last two decades, measurements of tensor-polarized observables, made possible by innovative accelerator and target technologies, have provided new experimental information to understand the electromagnetic structure of the deuteron [4–12] and put strong constraints on nuclear models, e.g., Hamiltonian dynamics [13,14], explicitly covariant models [15,16], as well as the latest developments in effective field theory for low-Q physics [17,18]. In this Letter, a high-precision measurement of the deuteron tensor analyzing powers T_{20} and T_{21} over a broad range of low-momentum transfer is reported.

In the one-photon exchange approximation, elastic electron scattering from the deuteron, a spin-1 nucleus, is completely described by three form factors, the charge monopole G_C, the quadrupole G_Q, and the magnetic dipole form factor G_M, which are only functions of the four-momentum transfer squared, Q^2. The unpolarized elastic electron-deuteron cross section σ_0 directly measures $S = A + B\tan^2(\theta_e/2)$ via $\sigma_0 = \sigma_{\text{Mott}} f_{\text{rec}}^{-1} S$, where $\sigma_{\text{Mott}} = (\alpha/2E)^2[\cos(\theta_e/2)/\sin^2(\theta_e/2)]^2$ is the Mott cross section and $f_{\text{rec}} = 1 + 2(E/M)\sin^2(\theta_e/2)$ is the nuclear recoil factor, with E and θ_e denoting the electron beam energy and scattering angle, respectively, and M the deuteron mass. Therefore, from measurements of σ_0 at two different angles and the same Q^2, two combinations of the deuteron form factors $A(Q^2) = G_C^2 + (8/9)\eta^2 G_Q^2 + (2/3)\eta G_M^2$ and $B(Q^2) = (4/3)\eta(1+\eta)G_M^2$, with $\eta = Q^2/(4M^2)$, can be derived. It requires at least one more independent measurement in order to separate the charge monopole and quadrupole form factors, G_C and G_Q. The additional measurement can be achieved with a tensor-polarized deuterium target, where the tensor-polarized cross section $\sigma = \sigma_0(1 + \frac{1}{\sqrt{2}} P_{zz} A_d^T)$ gives rise to a target tensor asymmetry

$$A_d^T = \frac{3\cos^2\theta^* - 1}{2} T_{20} - \sqrt{\frac{3}{2}} \sin 2\theta^* \cos\phi^* T_{21} + \sqrt{\frac{3}{2}} \sin^2\theta^* \cos 2\phi^* T_{22}. \quad (1)$$

Here, the polarization direction is described by the polar and azimuthal angles θ^* and ϕ^*, respectively, in a frame where the z axis is along the direction of the virtual photon and the y axis is defined by the vector product of the incoming and outgoing electron momenta. The quantity $P_{zz} = n_+ + n_- - 2n_0$ is the tensor polarization, where n_+, n_0, and n_- are the relative populations of the nuclear spin projections $m = +1, 0, -1$ along the direction of polarization, respectively. The tensor analyzing powers, T_{20}, T_{21}, and T_{22}, can be expressed as combinations of the three deuteron elastic form factors

$$T_{20}(Q^2, \theta_e) = -\frac{1}{\sqrt{2}S}\left[\frac{8}{3}\eta G_C G_Q + \frac{8}{9}\eta^2 G_Q^2 + \frac{1}{3}\eta\left(1 + 2(1+\eta)\tan^2\frac{\theta_e}{2}\right)G_M^2\right],$$

$$T_{21}(Q^2, \theta_e) = -\frac{2}{\sqrt{3}S}\sqrt{\eta^3\left(1 + \eta\sin^2\frac{\theta_e}{2}\right)} G_M G_Q \sec\frac{\theta_e}{2},$$

$$T_{22}(Q^2, \theta_e) = -\frac{1}{2\sqrt{3}S}\eta G_M^2. \quad (2)$$

Therefore, the measurement of tensor-polarized observables, combined with A and B, allows the determination of G_C, G_Q, and G_M. It is useful to consider the quantity $\tilde{T}_{20} = (T_{20} + \frac{\delta}{2\sqrt{2}})/(1 - \delta)$, in which the small correction by $\delta = [\frac{1}{2(1+\eta)} + \tan^2(\theta_e/2)]\frac{B}{S}$ eliminates the dependence on θ_e and G_M, resulting in

$$\tilde{T}_{20}(Q^2) = -\frac{\frac{8}{3}\eta G_C G_Q + \frac{8}{9}\eta^2 G_Q^2}{\sqrt{2}(G_C^2 + \frac{8}{9}\eta^2 G_Q^2)}, \quad (3)$$

which can be directly converted into the ratio G_C/G_Q. Dividing out the leading Q^2 dependence provides a reduced quantity $\tilde{T}_{20R}(Q^2) = -\frac{3}{\sqrt{2}Q_d Q^2}\tilde{T}_{20}(Q^2)$, in which details of the low-Q region are enhanced. The deuteron quadrupole moment is given by $Q_d = G_Q(0)/M^2 = 25.83/M^2 = 0.285\,783(30)$ fm^2 [19]; hence, with $G_C(0) = 1$, one has $\tilde{T}_{20R}(0) = 1$. The magnetic form factor is normalized as $G_M(0) = \mu_d M/M_N$, with $\mu_d = 0.857\,438\,230\,8(72)$ nuclear magnetons [20], where M_N is the nucleon mass.

Tensor-polarized observables can be measured as tensor moments of recoiling deuterons with unpolarized beam and target [4,8,11] or as tensor asymmetries with a tensor-polarized target [5–7,9,10,12]. The experiment reported in this Letter used a highly polarized deuterium gas target with a large acceptance magnetic spectrometer, which is different from all previous experiments.

The experiment was carried out with the Bates Large Acceptance Spectrometer Toroid (BLAST) in the South Hall Ring of the MIT-Bates Linear Accelerator Center; see [21,22] for details. An electron beam of up to 300 mA was stored with 65% longitudinal polarization preserved with a Siberian snake. The beam energy was 850 MeV, and the typical average current was 150 mA with a lifetime of about 20 minutes. Highly polarized atomic deuterium gas was generated by an atomic beam source in nuclear vector ($T+/V+$: $m = 1$; $T+/V-$: $m = -1$) and tensor ($T-$: $m = 0$) polarization states and injected into a 60 cm long, 15 mm diameter cylindrical windowless target storage cell cooled to 100 K and embedded in the ring vacuum [23]. A modest target holding magnetic field defined the polarization direction of the target spin. The target states were switched every 5 minutes by rf transition units in the atomic beam source. In addition, the helicity h of the electron beam was flipped every injection cycle.

The combination of polarized beam, polarized hydrogen, and vector-tensor-polarized deuterium target and a large acceptance spectrometer allowed asymmetry data to be collected simultaneously, over a large Q^2 range, in many reaction channels, such as $^1\vec{H}(\vec{e}, e'p)$ [24], $^2\vec{H}(\vec{e}, e'n)$ [25], $^2\vec{H}(\vec{e}, e'p)$, and $\vec{e}$-$\vec{d}$, e-$\overleftrightarrow{d}$ elastic scatterings [22]. The results and further impact from the latter reaction channel are reported here.

The large acceptance spectrometer [21] was built around eight copper coils providing a toroidal magnetic field of up to 3.8 kG around the beam line. The two horizontal sectors were instrumented with drift chambers for momentum, angular, and vertex reconstruction, covering polar angles between 20° and 80° and ±15° out of plane. Trigger and particle identification were provided by plastic time-of-flight (TOF) scintillators in each sector.

The elastic events were detected in coincidence, requiring one TOF hit and one charged particle to be reconstructed in the drift chamber in each sector. Three-σ cuts in angular and momentum correlation between the electrons and deuterons were used, taking advantage of the overdetermination of the elastic kinematics. Deuteron particle identification was based on TOF and kinematics, allowing for a very clean separation of protons and deuterons. The contamination by misidentified electrodisintegration events was estimated to be lower than 1%. Background due to beam halo scattered off the aluminum target cell wall was studied with the same target cell without gas or with hydrogen flowing through. The cell wall background was below 0.1% and negligible.

The target tensor asymmetry of Eq. (1) is derived experimentally as

$$A_d^T = \frac{\sqrt{2}}{P_{zz}}\frac{Y^+ - Y^-}{2Y^+ + Y^-}, \quad (4)$$

where Y^+ and Y^- are the charge-normalized yields with the target in the $T+$ ($m = \pm 1$) and the $T-$ ($m = 0$) state,

respectively. Two asymmetries were measured simultaneously corresponding to electrons scattered into the left and right sector.

Two sets of data were taken during late 2004 and early 2005. The integrated luminosities were 140 pb^{-1} and 340 pb^{-1}, corresponding to 370 kC and 560 kC integrated charge, respectively. The target spin was directed in the horizontal plane on average to 31.7° and 47.7° to the left side of the beam for the 2004 and 2005 data sets, respectively, each with about ±0.5° uncertainty. The spin angle in each case varied by a few degrees along the cell and was corrected using a carefully measured field map. The average spin angle was calibrated simultaneously with the target tensor polarization by comparing the elastic tensor asymmetries at low momentum transfer $1.75 < Q < 2.15\ \mathrm{fm}^{-1}$ to Monte Carlo simulations based on parametrization III [26] of previous experimental data. The uncertainty in the normalization is estimated to be ±5%, which is dominated by the dispersion between the three parametrizations [26]. The tensor polarizations for the 2004 and 2005 data sets were $P_{zz} = 0.683 \pm 0.015 \pm 0.013 \pm 0.034$ and $0.563 \pm 0.013 \pm 0.023 \pm 0.028$, respectively, where the three uncertainties are statistical, systematic, and due to the parametrization, in that order. The small T_{22} component in A_d^T was subtracted using the above parametrization, and T_{20} and T_{21} were extracted by solving the two-by-two linear equations relating the experimental asymmetries for electrons in the left and right sector of the detector and the two analyzing powers. For comparison to existing data, T_{20} and T_{21} have been adjusted to the conventionally accepted angle $\theta_e = 70°$. Table I and Fig. 1 show the results for T_{20} and T_{21} with statistical and total systematic uncertainties. The largest systematic uncertainty is due to the parametrization of world data in the calibration of P_{zz}. Other sources of systematic errors include the Q^2 determination, the spin orientation, and the statistical uncertainty in P_{zz}. In order to highlight the low-Q region, the values for T_{20} were converted to $\tilde{T}_{20R}$ using parametrization III [26] for δ; the results are depicted in Fig. 2.

The values for T_{20} measured in this work are in agreement with previous data; yet, they are much more precise. Our data cover a wide kinematic range, providing a strong constraint on the Q^2 evolution of T_{20} in an important region which contains the minimum of T_{20} and the first node of G_C. The T_{21} results are consistently larger in magnitude than all the models and previous measurements at high Q, albeit still consistent within the systematic errors.

The nonrelativistic model with meson exchange and relativistic corrections by Arenhövel *et al.* [13] agrees

TABLE I. T_{20} and T_{21} measured in this experiment and G_C and G_Q separated with present data and the structure function A. The upper errors for T_{20} and T_{21} are statistical, and the lower ones are systematic. Q is in fm^{-1}.

Q	T_{20}	T_{21}	G_C	G_Q
2.228	$-0.780^{\pm 0.021}_{\pm 0.053}$	$-0.149^{\pm 0.016}_{\pm 0.023}$	0.1223(14)	3.87(26)
2.404	$-0.877^{\pm 0.026}_{\pm 0.061}$	$-0.148^{\pm 0.023}_{\pm 0.030}$	0.0953(14)	2.99(20)
2.603	$-1.016^{\pm 0.031}_{\pm 0.076}$	$-0.224^{\pm 0.031}_{\pm 0.049}$	0.0701(17)	2.36(18)
2.827	$-1.172^{\pm 0.044}_{\pm 0.083}$	$-0.312^{\pm 0.050}_{\pm 0.064}$	0.0479(21)	1.84(15)
3.063	$-1.244^{\pm 0.051}_{\pm 0.086}$	$-0.433^{\pm 0.072}_{\pm 0.084}$	0.0314(33)	1.37(12)
3.319	$-1.251^{\pm 0.074}_{\pm 0.085}$	$-0.64^{\pm 0.12}_{\pm 0.10}$	0.0139(33)	1.091(55)
3.560	$-1.15^{\pm 0.10}_{\pm 0.08}$	$-0.57^{\pm 0.17}_{\pm 0.09}$	0.0087(26)	0.763(31)
3.823	$-1.13^{\pm 0.13}_{\pm 0.06}$	$-0.65^{\pm 0.21}_{\pm 0.08}$	0.0065(15)	0.522(24)
4.140	$-0.70^{\pm 0.17}_{\pm 0.05}$	$-0.74^{\pm 0.23}_{\pm 0.05}$	0.0003(17)	0.3637(48)

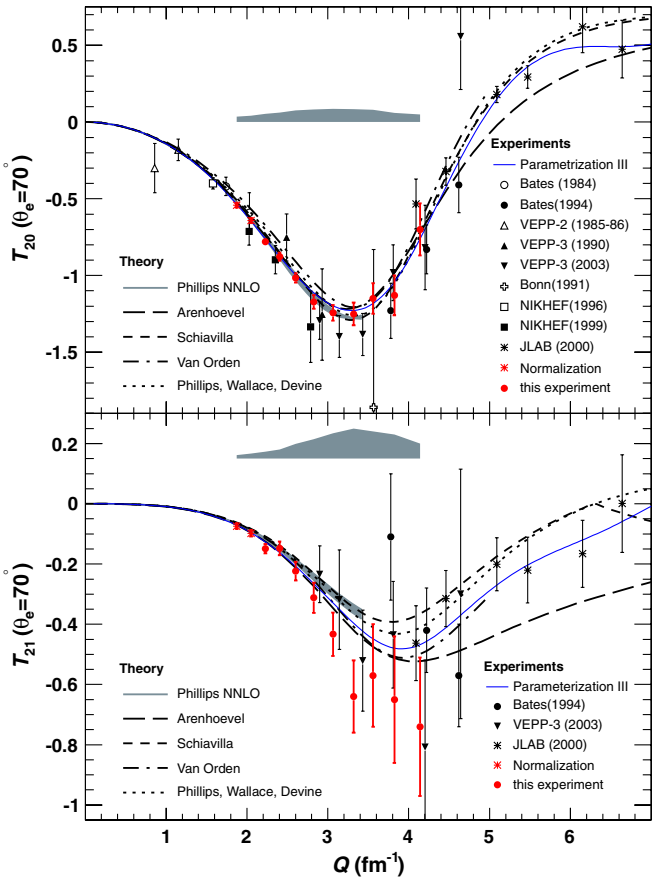

FIG. 1 (color online). Results for T_{20} and T_{21} [grey (red online) dots] compared to previous data [4] (open dots), [5,6] (open upright triangles), [7] (solid upright triangles), [8] (solid dots), [9] (open squares), [10] (solid squares), [11] (open stars), [12] (solid down triangles), and various theoretical predictions. The theoretical curves are nonrelativistic models with relativistic corrections [13] (long dashed line), [14] (dashed line), relativistic models [15] (dash-dotted line), [16] (dotted line), and effective field theory [17,18] (grey error band). Parametrization III [26], used for normalization, is shown (solid line) for reference. The shaded area represents the systematic uncertainties. The first two points at low Q [shown as grey (red online) stars] were used to calibrate polarization and spin angle, while the remaining nine points [shown as grey (red online) dots] represent new measurements.

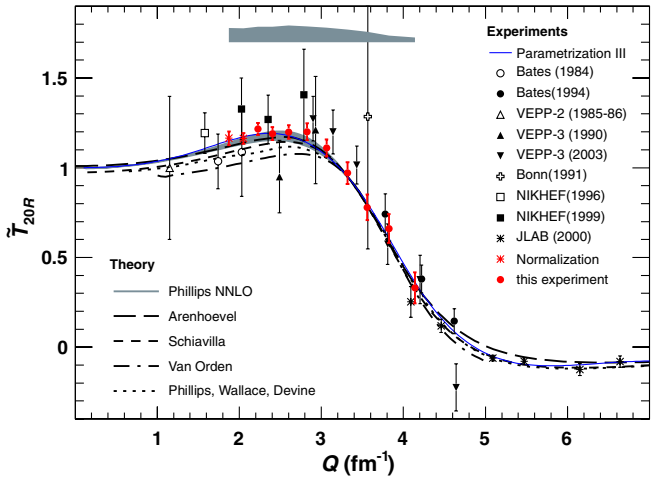

FIG. 2 (color online). Experimental results for $\tilde{T}_{20R}$ [grey (red online) symbols] in comparison with previous data and various theoretical predictions. Data and theoretical curves are labeled as in Fig. 1.

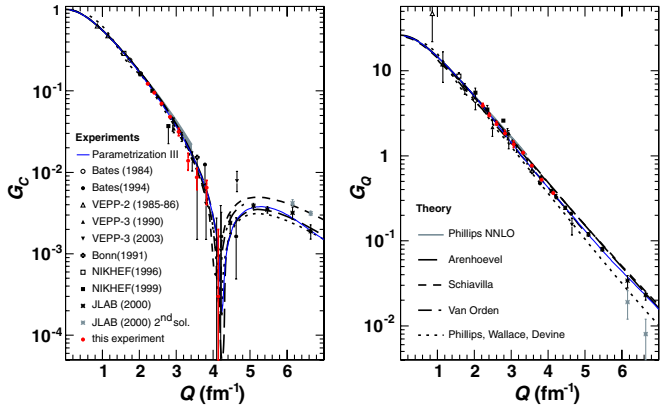

FIG. 3 (color online). Results for separated G_C and G_Q compared to various theoretical predictions. Curves and data are as in Fig. 1.

with our data very well, while it deviates from the experimental results of [11] at higher Q. Although the calculation by Schiavilla *et al.* [14] agrees with T_{20} measured in this work, it appears to underpredict the size of T_{21}. The relativistic calculation of T_{20} by Van Orden *et al.* [15] does not agree with our data at low Q even while T_{21} is in good agreement. The agreement improves at higher Q. The agreement is also much improved when our data are normalized to [15], which indicates a good prediction of the "shape" of T_{20}. An overall good description is given by the relativistic calculation of Phillips *et al.* [16].

The recent effective field theory (EFT) calculation by Phillips [17,18] in the framework of chiral perturbation theory is only valid below a momentum transfer of ≈ 3 fm^{-1}, up to which it agrees with our data very well. It should be noted that the quadrupole form factor G_Q plays an important role in both T_{20} and T_{21}; yet, none of the potential models [13–16] of G_Q reproduce the static deuteron quadrupole moment Q_d when extrapolated to $Q = 0$. This has been identified by the EFT calculation in [18] as a relativistic short-range effect, where the suggested renormalization leads to excellent agreement with our data, which can be best seen in Fig. 2.

The charge monopole and quadrupole form factors G_C and G_Q were separated for each Q value using existing data for structure function A, T_{20}, and T_{21} by minimizing the quantity

$$\chi^2 = \left[\frac{A - A^c}{\delta A}\right]^2 + \left[\frac{T_{20} - T_{20}^c}{\delta T_{20}^2}\right]^2 + \left[\frac{T_{21} - T_{21}^c}{\delta T_{21}}\right]^2, \quad (5)$$

in which T_{20} and T_{21} are the measured values and A^c, T_{20}^c, and T_{21}^c were calculated from G_C, G_Q, and G_M. In the fit, G_C and G_Q were varied while G_M and A were fixed by parametrization I [26]. The uncertainty in A was computed from the covariance matrix of the parametrization. The resulting values for G_C and G_Q are shown in Table I and Fig. 3.

The full parametrization I [26] of the deuteron form factors was refit with the results of Ref. [12] and of the present Letter included, and all 18 parameters, including the location of the first nodes of all three form factors, were allowed to vary. The fit confirms the location of the first node of G_C at 4.19 ± 0.05 fm^{-1}, consistent with previous findings [12,26].

In conclusion, we have measured the deuteron tensor analyzing powers in the momentum transfer range of 2.15 to 4.50 fm^{-1}. Our results are consistent with previous data, yet with much improved precision. The wide kinematic coverage provides unique information on the Q dependence of T_{20} and T_{21}. Our data are in excellent agreement with recent results in the EFT framework, which offers a solution for the long-standing problem of the deuteron quadrupole moment. Our data have enabled the separation of the deuteron form factors G_C and G_Q in the low Q region and have confirmed the location of the first node of G_C.

We thank the staff at the MIT-Bates Linear Accelerator Center for the delivery of a high-quality electron beam and their technical support. We also thank H. Arenhövel, R. Gilman, D. Nikolenko, D. R. Phillips, and J. W. Van Orden for many enlightening discussions. This work has been supported in part by the U.S. Department of Energy and the National Science Foundation.

*Corresponding author.
kohlm@jlab.org

[1] J. Carlson and R. Schiavilla, Rev. Mod. Phys. **70**, 743 (1998).
[2] M. Garçon and J. W. Van Orden, Adv. Nucl. Phys. **26**, 293 (2002).
[3] R. Gilman and F. Gross, J. Phys. G **28**, R37 (2002).

[4] M. E. Schulze *et al.*, Phys. Rev. Lett. **52**, 597 (1984).
[5] V. F. Dmitriev *et al.*, Phys. Lett. **157B**, 143 (1985).
[6] B. B. Wojtsekhowski *et al.*, Pis'ma Zh. Eksp. Teor. Fiz. **43**, 567 (1986) {JETP Lett. **43**, 733 (1986) [http://www.jetpletters.ac.ru/ps/1413/article_21505.shtml]}.
[7] R. Gilman *et al.*, Phys. Rev. Lett. **65**, 1733 (1990).
[8] I. The *et al.*, Phys. Rev. Lett. **67**, 173 (1991).
[9] M. Ferro-Luzzi *et al.*, Phys. Rev. Lett. **77**, 2630 (1996).
[10] M. Bouwhuis *et al.*, Phys. Rev. Lett. **82**, 3755 (1999).
[11] D. Abbott *et al.*, Phys. Rev. Lett. **84**, 5053 (2000).
[12] D. M. Nikolenko *et al.*, Phys. Rev. Lett. **90**, 072501 (2003).
[13] H. Arenhövel, F. Ritz, and Th. Wilbois, Phys. Rev. C **61**, 034002 (2000).
[14] R. Schiavilla and V. R. Pandharipande, Phys. Rev. C **65**, 064009 (2002).
[15] J. W. Van Orden, N. Devine, and F. Gross, Phys. Rev. Lett. **75**, 4369 (1995).
[16] D. R. Phillips, S. J. Wallace, and N. K. Devine, Phys. Rev. C **58**, 2261 (1998).
[17] D. R. Phillips, Phys. Lett. B **567**, 12 (2003).
[18] D. R. Phillips, J. Phys. G **34**, 365 (2007).
[19] M. Pavanello, W.-C. Tung, and L. Adamowicz, Phys. Rev. A **81**, 042526 (2010).
[20] P. J. Mohr, B. N. Taylor, and D. B. Newell, Rev. Mod. Phys. **80**, 633 (2008).
[21] D. Hasell *et al.*, Nucl. Instrum. Methods Phys. Res., Sect. A **603**, 247 (2009).
[22] D. Hasell *et al.*, Annu. Rev. Nucl. Part. Sci. **61**, 409 (2011).
[23] D. Cheever *et al.*, Nucl. Instrum. Methods Phys. Res., Sect. A **556**, 410 (2006).
[24] C. B. Crawford *et al.*, Phys. Rev. Lett. **98**, 052301 (2007).
[25] E. Geis *et al.*, Phys. Rev. Lett. **101**, 042501 (2008).
[26] D. Abbott *et al.*, Eur. Phys. J. A **7**, 421 (2000).